Final Report Cover Sheet

DOE Program: DE-PS02-09ER09-21 Computational Science Research for Ice Sheet Modeling

DOE award *#DE-SC0002137* awarded to Columbia University

Modeling the Fracture of Ice Sheets on Parallel Computers

Lead Institution: Columbia University (CU), PI: Haim Waisman

Collaborating Institution: Sandia National Labs (SNL), PI: Ray Tuminaro

DOE program manager: Randall Laviolette (Randall.Laviolette@science.doe.gov)

Submission Date: September 10, 2013
Report Period: 09/15/10 to 09/14/13

Principal Investigator:

Haim Waisman, Assistant Professor
Department of Civil Engineering & Engineering Mechanics
Columbia University
624 S.W. Mudd Building
500 West 120th Street
New York, NY 10027
Tel: (212) 851-0408
Fax: (212) 854-6267
waisman@civil.columbia.edu

Contents

Modeling the Fracture of Ice Sheets on Parallel Computers

Haim Waisman, David Keyes
School of Engineering and Applied Science, Columbia University, New York, NY

Ray Tuminaro, Erik Boman
Sandia National Laboratories, Albuquerque, NM

1 Objectives and Accomplishments (Sep 15, 2009-Sep 14, 2013)

The objective of this project was to investigate the complex fracture of ice and understand its role within larger ice sheet simulations and global climate change. This objective was achieved by developing novel physics based models for ice, novel numerical tools to enable the modeling of the physics and by collaboration with the ice community experts.

Fracture of ice is important in several fields of which the most visible and certainly the most significant is global warming. This has recently received international attention due to the collapse of some significant ice shelves [1, 2, 3]. Ice fracture, however, is also important in other areas including oil and gas exploration and production within ice-infested waters [4, 5], materials science research and length scales in ice [6, 7] and microbiology [8].

At the present time, ice fracture is not explicitly considered within ice sheet models due in part to large computational costs associated with the accurate modeling of this complex phenomena. However, fracture not only plays an extremely important role in regional behavior but also influences ice dynamics over much larger zones in ways that are currently not well understood. Dramatic illustrations of fracture-induced phenomena most notably include the recent collapse of ice shelves in Antarctica (e.g. partial collapse of the Wilkins shelf in March of 2008 and the diminishing extent of the Larsen B shelf from 1998 to 2002).

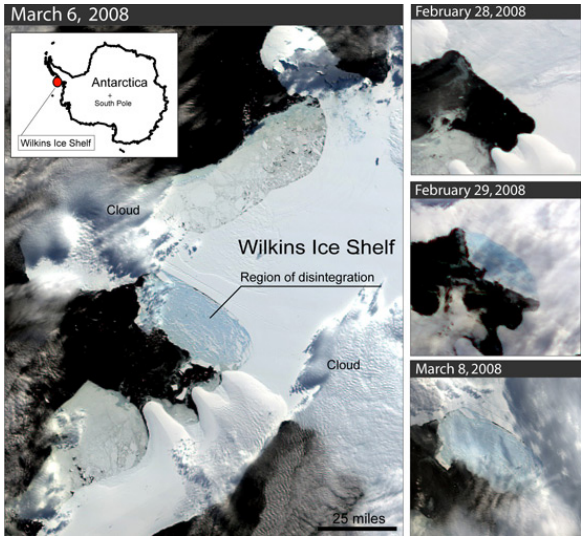

(b) Wilkins ice shelf

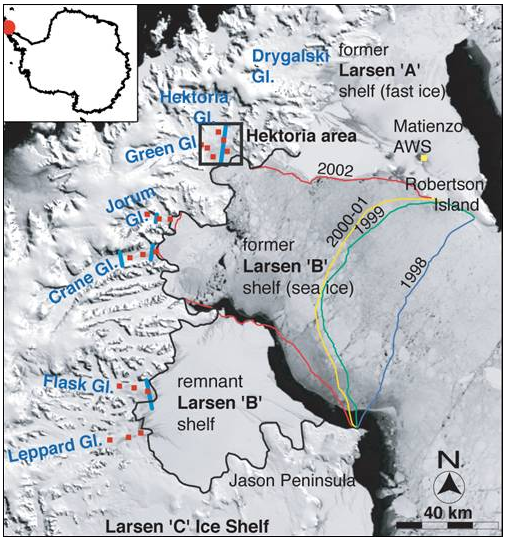

(c) Larsen B diminishing shelf

Figure 1: Recent collapse of ice shelves in Antarctica

Other fracture examples include ice calving (fracture of icebergs) which is presently approxi-

mated in simplistic ways within ice sheet models, and the draining of supraglacial lakes through a complex network of cracks, a so called *ice sheet plumbing system*, that is believed to cause accelerated ice sheet flows due essentially to lubrication of the contact surface with the ground. These dramatic changes are emblematic of the ongoing change in the Earth's polar regions and highlight the important role of fracturing ice.

To this end, our research findings through this project offers significant advancement to the field and closes a large gap of knowledge in understanding and modeling the fracture of ice sheets in the polar regions. Thus, we believe that our objective has been achieved and our research accomplishments are significant. This is corroborated through a set of published papers, posters and presentations at technical conferences in the field. In particular significant progress has been made in the mechanics of ice [9, 10, 11], fracture of ice sheets and ice shelves in polar regions [12, 13, 14] and sophisticated numerical methods that enable the solution of the physics in an efficient way [15, 16, 17, 18].

2 Collaborations between Columbia University, Sandia National Labs and the ice community

The collaborating groups from Columbia University and Sandia National Labs have had very good interactions during the past four years of the project. The team held conference calls to exchange and share research ideas, results, administrative issues concerning the project, hiring staff, etc. We have also had code exchanges to explore ideas on the same platform. The groups hired two postdoctoral fellows (Dr. Axel Gerstenberger who was located at Sandia Albuquerque and currently is back in Germany and Dr. Ravindra Duddu who was located at Columbia University and currently an assistant professor at Vanderbilt University. The hiring was coordinated by both teams so that the work objectives of the postdocs was complementary and inline with the project goals.

Throughout the project co-PI Ray Tuminaro visited Columbia University, attended joint meetings and served on a PhD committee for Badri Hiriyur (former student at Columbia University and currently at Weidlinger Associates Inc.). Similarly, co PIs Haim Waisman and David Keyes visited at Sandia Labs in Livermore, CA to enhance collaboration and discuss research activities related to this project. Two students from Columbia University interned several summers at Sandia Albuquerque and Livermore to enhance the collaboration between the groups. The teams also met at conferences, e.g. the International Congress on Industrial & Applied Mathematics which was held in July 2011 (ICIAM 2011). During these meetings we discussed technical issues related to the project and other aspects of the project.

This project period has led to a truly fruitful collaboration with several important journal papers published, conference proceedings, posters and presentations at various conferences for example: Domain Decomposition 2011, Copper Mountain Conference on Multigrid Methods 2011, Land Ice Working Group 2011 (at Boulder CO), United States Computational Mechanics Conference 2011 (at Miniannapolis, MN), XFEM 2011 conference (at Cardiff University, UK), Engineering Mechanics Institute 2011 (at Boston MA), International Congress on Industrial & Applied Mathematics 2011 (Vancouver, BC, Canada), American Geophysical Union 2012, Engineering Mechanics Institute conference 2012 (Boston, MA) and World Congress on Computational Mechanics 2012 (Sao Paulo, Brazil).

It is also important to mention the interaction of the team with the ice modeling community. In particular the team had several idea exchanges with Dr. Bill Lipscomb (LANL) and Dr. Jeremy

Bassis (U. of Michigan). Partial data given to the group (by Dr. Bassis) has allowed us to generate the mesh for the Amery ice shelf (located in Antarctica) as illustrated in Figure 2.

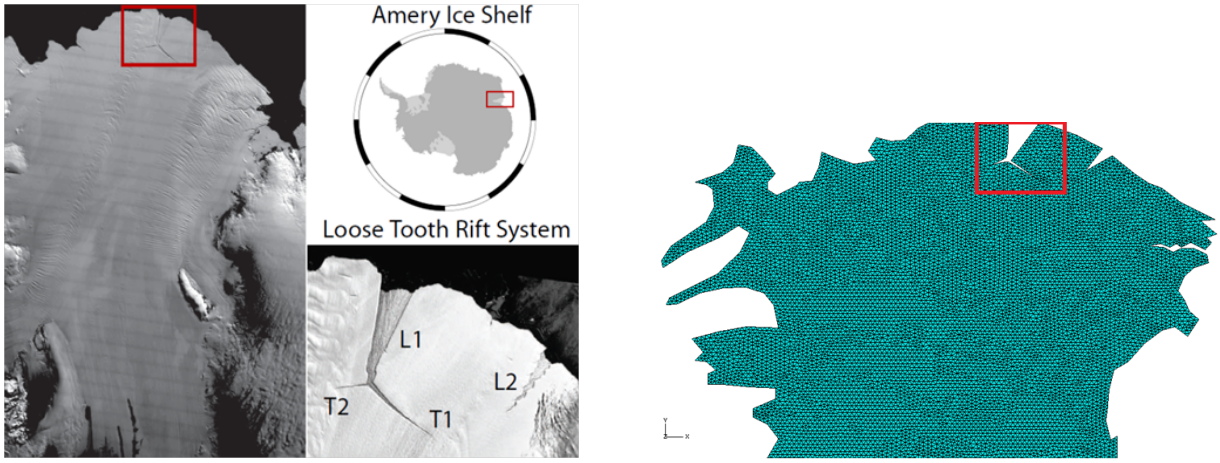

(a) Satellite image showing giant rifts

(b) Finite Element Mesh

Figure 2: Amery ice shelf in Antarctica

Moreover, the Columbia team continued to work closely with Dr. Jeremy Bassis, which recently resulted in a paper on the numerical investigation of surface crevasse propagation in glaciers and published by the Geophysics Research Letters [12] and poster presentations at the American Geophysics Union fall meeting in 2012 [14] and the World Climate Research Programme Open Science Meeting in 2012 [13].

We note that the collaboration with the ice community has also led to a couple of NSF proposals (one is currently pending) that were based on this project and expand some of the research ideas to tackle more interesting work in fracture of ice.

3 Research accomplishments

The collaborating groups from Columbia University (Haim Waisman and David Keyes) and Sandia National Labs (Ray Tuminaro and Erik Boman) have made significant progress since the starting date of this project (Sep. 15, 2009), in three main directions inline with our statement of work: (i) material models of ice and fracture of ice sheets and ice shelves, coupled with global warming effects (4 papers have been published [9, 10, 12, 11]) (ii) extended finite element methods for modeling the fracture [19, 20, 21, 22], and (iii) sophisticated algebraic multigrid techniques to solve the resulting systems robustly and efficiently [16, 15, 17, 18]. The next subsections briefly summarizes our progress. Full details can be found in the references provided.

3.1 A temperature dependent creep damage model for polycrystalline ice

Understanding the temperature dependent creep response of ice under a multiaxial state of stress is crucial for modeling the flow and deformation of glaciers, ice shelves and ice sheets. The material response of ice is highly nonlinear, viscoelastic, and anisotropic. The response depends

mainly on: the applied stress, the strain-rate, the temperature, the salinity, the porosity, the grain-size, the external pressure, and the anisotropic effect of ice. Further, the creep response of ice at later stages (tertiary creep) is enhanced due to the gradual accumulation of microcracks (damage) with time. Experiments by Jacka [23] suggest that both the viscous strain rate and the damage accumulation rate of ice are temperature dependent. Therefore, it is important that the material model for polycrystalline ice is able to capture the dependence of creep response on temperature in addition to strain-rate, external pressure, microcracking, etc.

The behavior of undamaged polycrystalline ice is assumed to be isotropic and viscoelastic owing to the random orientation of its crystalline structure. Assuming small strains, the additive decomposition of the total strain tensor into its components is assumed as,

$$\varepsilon_{kl} = \varepsilon^e_{kl} + \varepsilon^d_{kl} + \varepsilon^v_{kl}, \tag{1}$$

where $\varepsilon^e_{kl}, \varepsilon^d_{kl}$ and ε^v_{kl} denote the elastic, delayed elastic, and viscous strain tensors. Throughout this article we use the standard summation convention for repeated indices. The elastic stress-strain relation is given by the generalized Hooke's law,

$$\sigma_{ij} = C^e_{ijkl}\varepsilon^e_{kl}, \tag{2}$$

where σ_{ij} is the Cauchy stress tensor and C^e_{ijkl} is the fourth order "Elasticity" tensor. The Young's modulus of ice, generally derived from acoustic velocity measurements on ice specimens, depends strongly on its density and slightly on temperature [24]. The Young's modulus of laboratory ice is observed to increase by 5% in the range of -38°C to 0°C from 8.93 to 9.39 GPa and the Poisson's ratio is observed to increase by about 1% in the same temperature range. For engineering purposes these temperature dependencies may be described by simple linear relations [24]. The delayed elastic strain rate, $\dot{\varepsilon}^d_{kl} = \dfrac{\partial \varepsilon^d_{kl}}{\partial t}$, is given by [25],

$$\dot{\varepsilon}^d_{kl} = A\left(\frac{3}{2}K\sigma^{\text{dev}}_{kl} - \varepsilon^d_{kl}\right), \tag{3}$$

where A and K are material constants, and

$$\sigma^{\text{dev}}_{kl} = \sigma_{kl} - \frac{1}{3}\sigma_{ii}\delta_{kl}, \tag{4}$$

is the deviatoric part of the Cauchy stress. The permanent viscous strain rate, $\dot{\varepsilon^v}_{kl}$, is generalized by the power-law creep equation as,

$$\dot{\varepsilon^v}_{kl} = \frac{3}{2}K_N\left(\frac{3}{2}\sigma^{\text{dev}}_{mn}\sigma^{\text{dev}}_{mn}\right)^{(N-1)/2}\sigma^{\text{dev}}_{kl}. \tag{5}$$

where K_N and N are viscous parameters. The dependence of the viscosity coefficient, K_N, on temperature, T, is given by an Arrhenius type relation,

$$K_N(T) = K_N(T_m)\exp\left(\frac{-Q}{R}\left(\frac{1}{T} - \frac{1}{T_m}\right)\right). \tag{6}$$

where Q is the creep activation energy, R is the universal gas constant (which is equal to the Boltzmann's constant) and $K_N(T_m)$ is the viscosity coefficient at temperature, T_m. The equations (1)-(6) establish the generalized viscoelastic constitutive relations for undamaged, homogenous, and isotropic polycrystalline ice.

Remark 1 *The creep rate equation given by (5) is a multi-axial generalization of the power-law creep equation for the uniaxial case given by,*

$$\dot{\varepsilon} = K_0 \sigma^N \exp\left(\frac{-Q}{RT}\right). \tag{7}$$

where K_0 is a constant and σ is the constant uniaxial stress. In the glaciological literature this equation is known as the Glen's creep law for ice [26]. The power exponent, N, is determined to be ≈ 3 in most experimental and field investigations.

3.1.1 Damage evolution law

The damage evolution law describes the growth of damage that leads to eventual failure of the material. An appropriate damage evolution law for ice should be able describe: (i) multi-axial behavior (ii) different failure behavior in tension, compression and shear (iii) temperature dependence (iv) damage induced anisotropy (v) healing. Typically, in most engineering materials damage is an irreversible process, but, when it comes to ice damage is reversible due to recrystallization (healing). This is because the melting or freezing point of ice ($0^{\circ}\mathrm{C}$) is much lower than most engineering materials such as metals and polymers. However, we shall not consider healing in the current model due to the lack of detailed experimental investigations of healing in ice. The present temperature dependent creep damage model is based on the anisotropic damage theory given in [27].

Rate of damage: In a Lagrangian framework assuming small strains, the damage evolution rate, $\dot{D}_{ij} = \dfrac{\partial D_{ij}}{\partial t}$, is given by,

$$\dot{D}_{ij} = \begin{cases} f_{ij}, & \text{if} \quad \varepsilon_{ij} \geq \varepsilon_{th}, \\ 0, & \text{if} \quad \varepsilon_{ij} < \varepsilon_{th}, \end{cases} \tag{8}$$

where $f_{ij}(\boldsymbol{\sigma}, T, \mathbf{D})$ is the damage evolution function that depends on the Cauchy stress tensor, $\boldsymbol{\sigma}$, on the temperature, T, and on the damage tensor, $\mathbf{D}$; and ε_{th} is a strain threshold for damage initiation.

Remark 2 *The function, $\boldsymbol{f}$, also depends on the macroscopic density of ice, ρ [28]. Since the damage variable, $\mathbf{D}$, represents an equivalent porosity, the variations in density due to variations in porosity may be accounted by imposing some initial conditions on the damage variable, $\mathbf{D}$, or on the Young's modulus, E. The function, $\boldsymbol{f}$ should depend on $\mathbf{D}$ since the presence of existing damage reduces the potential sites for nucleation and growth. For laboratory grown ice the initial condition is generally taken to be $\mathbf{D}(t) = \mathbf{0}$.*

Strain threshold: The strain threshold is a mesoscale parameter proposed here to model the experimentally observed behavior of ice given in [29, 23]. A general form of the scalar creep damage evolution function, f, for isotropic damage and uniaxial loading is,

$$f = B\, \sigma^r\, (1-d)^{-k}, \tag{9}$$

where B, r, k are the damage evolution parameters, d is the scalar isotropic damage variable, and σ is the applied uniaxial stress. Later, Murakami and Ohno [30] generalized this model for multiaxial loading and orthotropic damage by replacing σ with the Hayhurst criterion and d with a second-order tensor damage variable, D. This generalized form of $\boldsymbol{f}$ is given by,

$$\begin{aligned} f_{ij}(\boldsymbol{\sigma}, T, \mathbf{D}) &= B(T)\ \langle\langle \chi(\tilde{\boldsymbol{\sigma}})\rangle\rangle^r\ (\omega_{kk})^{k(\sigma_{ij})} \left[(1-\gamma)\delta_{ij} + \gamma \xi_i^{(1)} \xi_j^{(1)}\right], \\ \chi(\tilde{\boldsymbol{\sigma}}) &= \alpha \tilde{\sigma}^{(1)} + \beta \sqrt{\frac{3}{2} \tilde{\sigma}_{mn}^{\mathrm{dev}} \tilde{\sigma}_{mn}^{\mathrm{dev}}} + (1-\alpha-\beta)\tilde{\sigma}_{kk}, \end{aligned} \tag{10}$$

where α, β are the material parameters; $\tilde{\sigma}^{(1)}$ is the maximum eigenvalue of $\tilde{\boldsymbol{\sigma}}$; $\boldsymbol{\xi}^{(1)}$ is the eigenvector associated with $\tilde{\sigma}^{(1)}$; χ is an equivalent stress measure. The function $\langle\langle \chi \rangle\rangle$ is defined as,

$$\langle\langle \chi \rangle\rangle = \begin{cases} \chi, & \text{if} \quad \chi \geq 0, \\ 0, & \text{if} \quad \chi < 0. \end{cases} \tag{11}$$

Remark 3 *The equivalent stress measure, χ, is a linear combination of the effective maximum principal stress, $\tilde{\sigma}^{(1)}$, the first invariant, $\boldsymbol{I}_{\tilde{\boldsymbol{\sigma}}} = \tilde{\sigma}_{kk}$ of the effective stress tensor, $\tilde{\boldsymbol{\sigma}}$, and the second invariant, $\boldsymbol{II}_{\boldsymbol{\sigma}^{dev}} = \frac{1}{2}\tilde{\sigma}_{mn}^{\mathrm{dev}}\tilde{\sigma}_{mn}^{\mathrm{dev}}$, of the deviatoric part of the effective stress tensor, $\tilde{\boldsymbol{\sigma}}^{dev}$.*

3.1.2 Model calibration and Model predictions

In this subsection we briefly present a few calibration and prediction results as compared with published experiments.

Uniaxial tension at $T = -10^{\circ}\mathrm{C}$: Experiments on laboratory grown ice samples were performed by Mahrenholtz and Wu [31] at $T = -10^{\circ}\mathrm{C}$ for three different values of uniaxial tension, $\sigma = 0.93,\ 0.82,\ 0.64$ MPa. Using this experimental data the viscosity and damage parameters in tension are calibrated at $T = -10^{\circ}\mathrm{C}$ (see Figure 4).

Uniaxial compression at $T = -5^{\circ}\mathrm{C}$: Experiments on laboratory grown ice samples were performed by Mellor & Cole [29] at $T = -5^{\circ}\mathrm{C}$ for a range of uniaxial compressive loading, $\sigma = 1-4$ MPa. Using this experimental data the viscosity and damage parameters in compression are calibrated at $T = -5^{\circ}\mathrm{C}$ (see Figure 8). The experimental data coordinates shown in Figure 8 are obtained by measuring the plots in [29]. The viscosity coefficient, K_N, is assumed from [25]. The damage parameters, B and k are calibrated by fitting the data of log-log plots of strain rate vs strain when the strains are greater than 1%. The parameter, k, calibrated here works for low stress, $3.06 < |\sigma| < 0.6$ MPa. For higher compressive stresses ($|\sigma| > 3.06$ MPa), we shall assume, $k = 0$, owing to the lack of experimental data. The experiments on ice under compression do not suggest any critical damage condition and the failure is ductile. The parameters are Hayhurst's criterion are assumed as $\alpha = 0.0$ and $\beta = 0.84$.

Discussion The behavior of material ice is complex and it dependent on many factors. The proposed model is based on idealized material laws namely: the Glen's creep law, Murakami's damage evolution law and the Arrhenius law for temperature dependence. This model does not

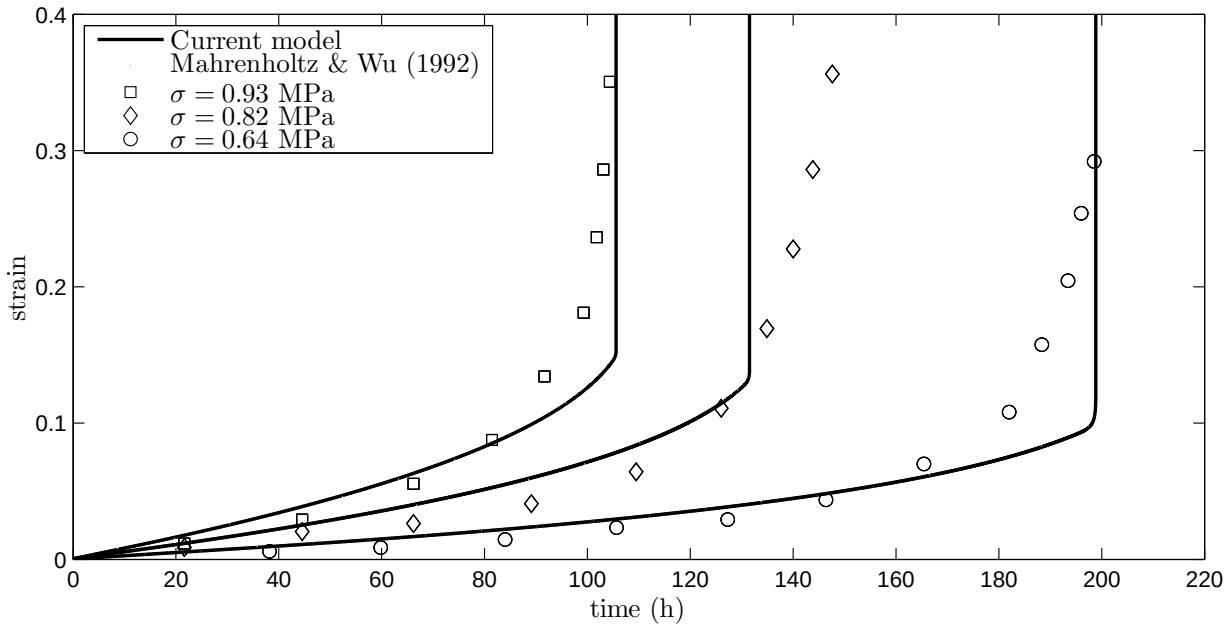

(a) Time evolution of strain

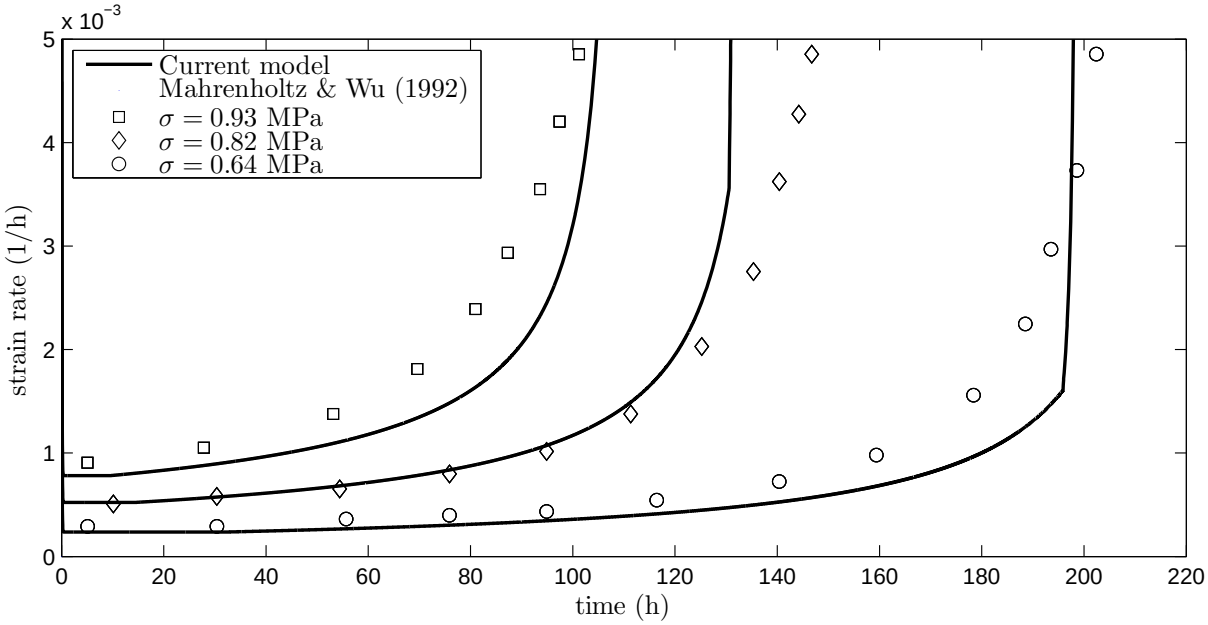

(b) Time evolution of strain rate

Figure 3: Uniaxial tension data of [31] used to identify the damage evolution parameters and their corresponding fits.

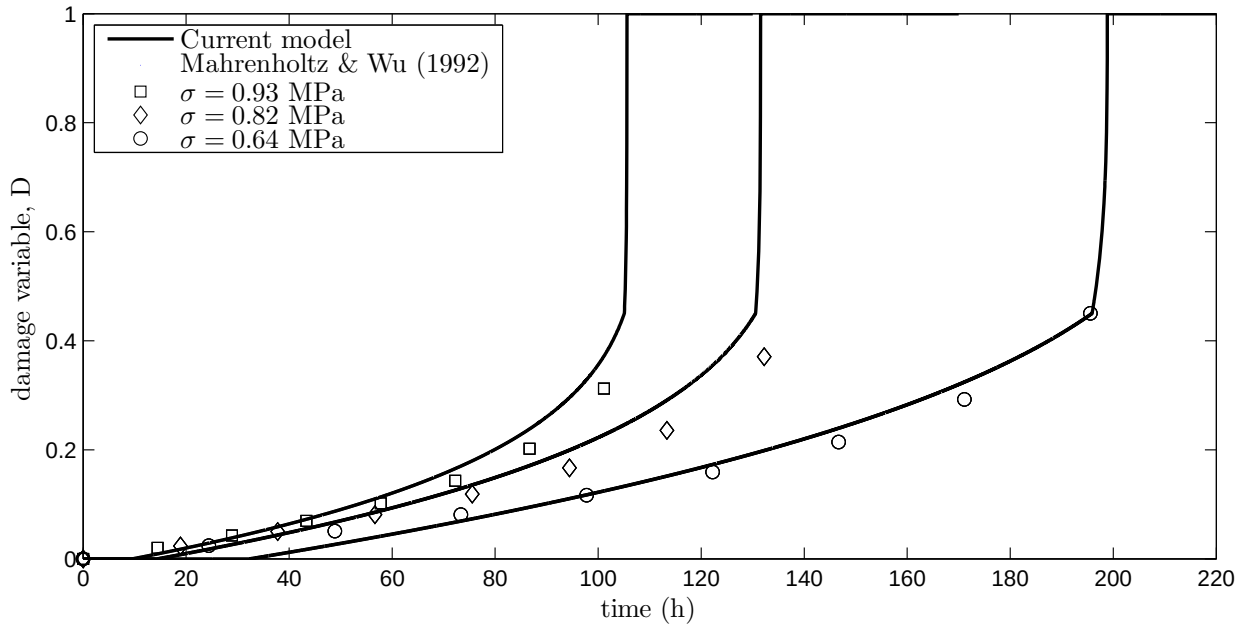

(a) Time evolution of damage

Figure 4: Uniaxial tension data of [31] used to identify the damage evolution parameters and their corresponding fits.

consider the strong dependence of material properties on grain size and density. The parameters evaluated in compression from data in [29, 23] are different probably because the values of grain size and density of ice reported in these studies are different from one another. More detailed and accurate experiments are needed to include the dependencies on grain-size and density. We note that the proposed model for ice is only applicable for low stresses and deformation rates which is often the case for ice in polar regions.

Model Predictions In this paragraph we briefly present some of the model predictions for uniaxial and multi-axial loading. The model predictions match well with experimental and numerical results in the literature. The numerical examples considered here illustrate the viability of the model for studying failure of ice-sheets occurring at low strain rates. The model results for uniaxial compression at low applied strain rates at $T = -5^{\circ}\mathrm{C}$ (see Figure 10(a)) match well with those in [29]. The results diverge for high strain rates ($> 10^{-5}$) because the Glen's creep exponent, N, increases with strain rate. The results at low strain rates show that ice strength is lower in tension than compression (see Figure 10(b)). The results also capture the ductile behavior of ice under tension at low strain rates.

3.1.3 Application of the nonlocal continuum damage mechanics to investigate surface crevasse propagation in glaciers

We use the nonlocal viscoelastic damage model to investigate the conditions that enable water-free surface crevasse propagation in grounded marine terminating glaciers. Our simulations, on idealized rectangular ice slabs in contact with the ocean, show that crevasses propagate faster

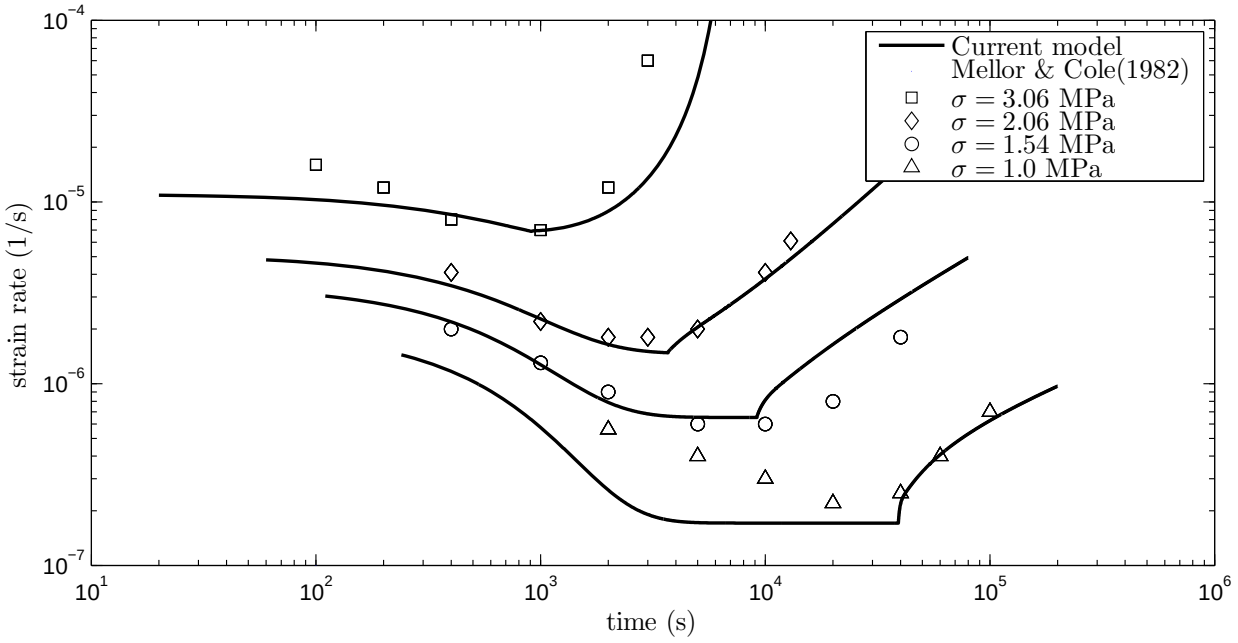

(a) Time evolution of strain rate

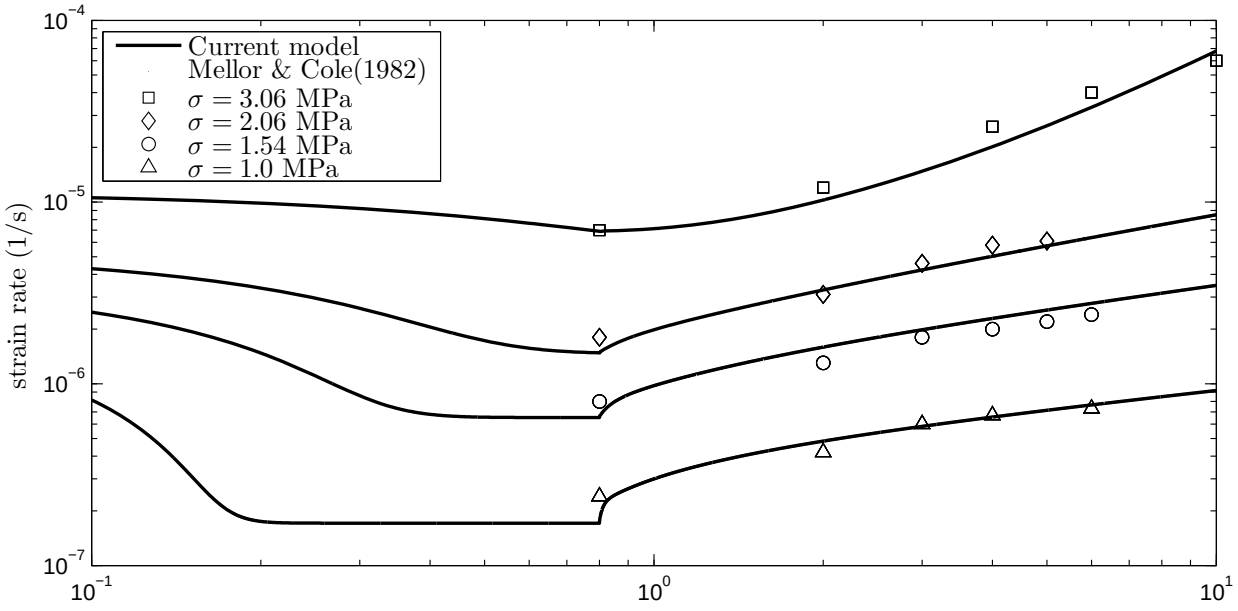

(b) Evolution of strain rate with strain

Figure 5: Uniaxial compression data of [29] used to identify the damage evolution parameters and their corresponding fits.

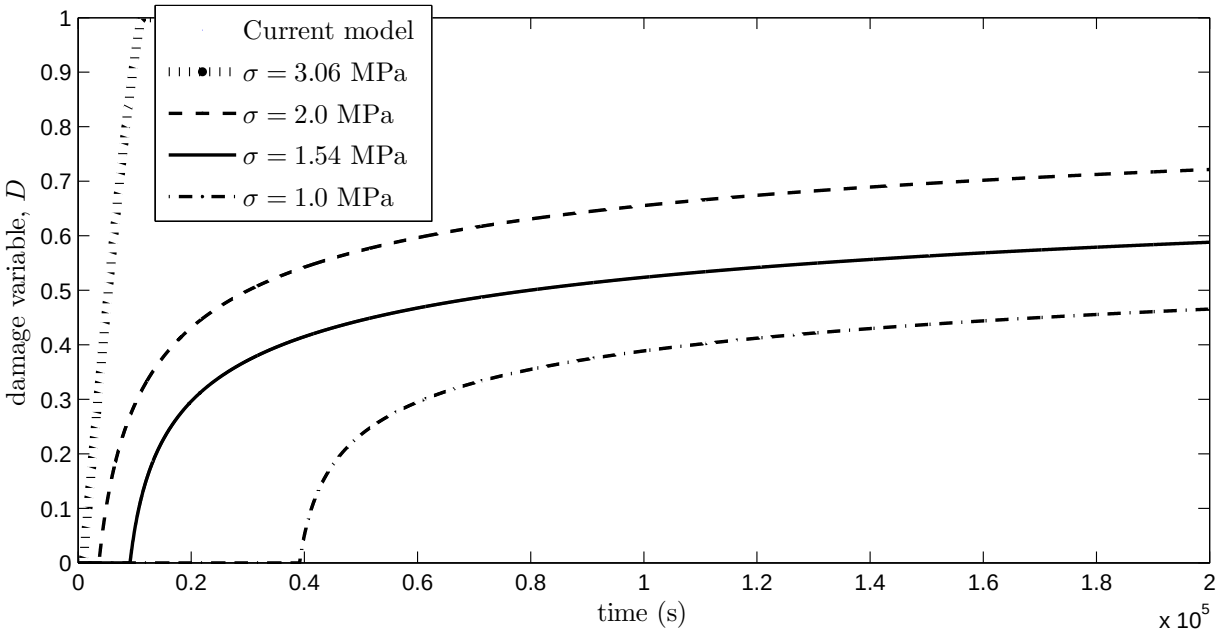

(a) Time evolution of damage

Figure 6: Uniaxial compression data of [29] used to identify the damage evolution parameters and their corresponding fits.

in thicker ice slabs. We find that: (1) the fraction of ice slab thickness penetrated by surface crevasses decreases with increasing seawater depth near the terminus; (2) a no slip (fixed) basal boundary condition retards crevasse growth; (3) crevasses form closer to the terminus when the seawater depth is larger or when the glacier base is fixed to the bedrock, which could lead to calving of smaller icebergs. However, water-free surface crevasses can penetrate (nearly) the entire ice thickness only in thicker ice slabs terminating in shallow seawater depths. This leads us to the conclusion that surface crevasses alone are not responsible for calving events in marine terminating and thin glaciers.

Crevasse propagation in a dry environment We first investigated the influence of ice thickness on calving in a dry environment ($h_w = 0$) by performing simulations with ice slabs thicknesses $h = 125, 250, 500$ m. In each case, we prescribe a notch of depth $d = 10$ m at mid-length near the glacier's top surface to initialize the crevasse. We take the slab length $l = 4h$ (in all the simulations) so that it is sufficiently long to develop the tensile stresses at mid-length, due to differential creep flow of the slab across the thickness. Figure 8 shows a crevasse opening within the contour plots of the horizontal displacement for the thickest glacier ($h = 500$ m) computed using a free slip basal boundary condition. The surface crevasse penetrates (nearly) the entire ice thickness over a period of approximately 33 hours (≈ 1.5 days).

Figure 9 shows normalized crack length to slab thickness versus time curves. Simulations suggest that crevasses propagate much faster and penetrate to greater depths in thicker ice slabs, which is in agreement with the theoretical findings of [32]. However, we are faced with the conundrum that crevasses only penetrate (nearly) the entire ice thickness for the thickest slabs ($h = 500$ m)

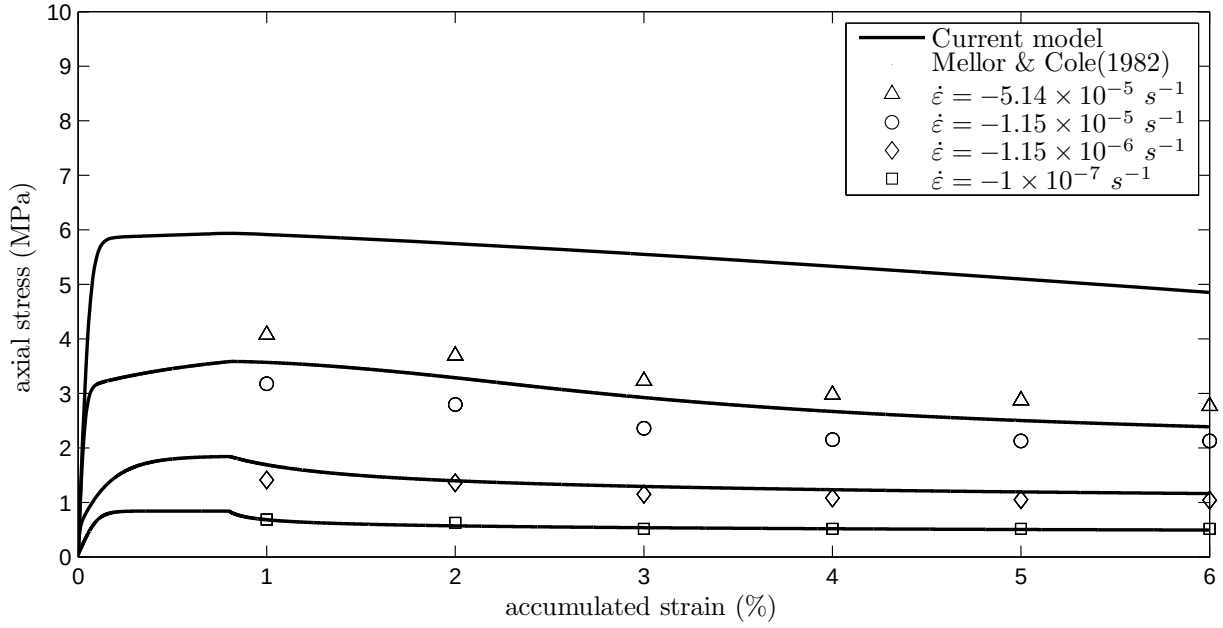

(a) Ductile behavior of ice under compression

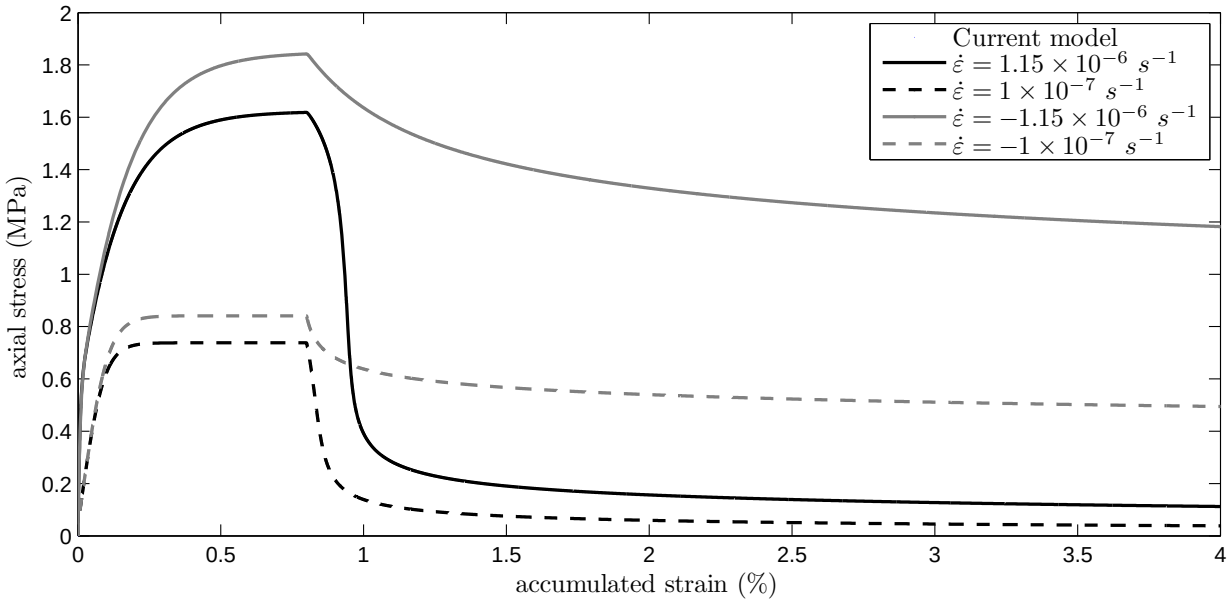

(b) Behavior of ice under tension and compression at low strain rates

Figure 7: Uniaxial behavior at $T = -5°\mathrm{C}$ at the constant strain-rate predicted by the model. The experimental data at the corresponding strain rates from [29] is plotted in (a). The model predictions match well with the experimental data.

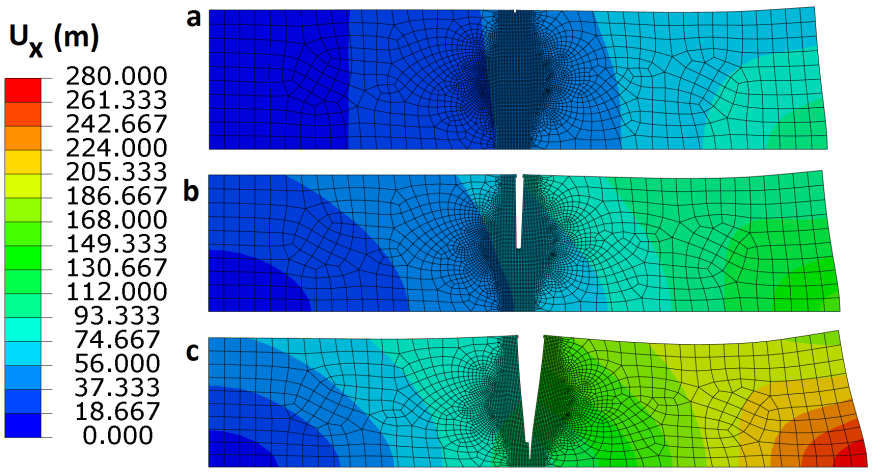

Figure 8: Contour plots of the displacement component in x direction (in meters) showing crevasse opening at times: (a) t = 16 hours; (b) t = 22 hours; (c) t = 33 hours. Depth varying flow velocity field is evident from these plots particularly near the terminus. The deformations and crack opening displacements are not drawn to scale.

whilst observations indicate that calving occurs for much smaller ice thicknesses [33, 32]. This suggests that additional mechanisms, such as meltwater enhanced hydrofracture, basal crevassing or shear failure must be considered to explain full thickness failure.

Influence of seawater depth and basal boundary condition Next, we estimated the depth to which surface crevasses penetrate in a marine terminating glacier as a function of water depth and ice thickness. The problem set up is similar to that described in the previous section. The water depth to slab thickness ratio (h_w/h) is varied from 0 to 0.8 (corresponding to a range that varies from fully grounded to near floatation) and the corresponding surface crevasse penetration ratios (d/h) obtained are shown in Figure 10. The results indicate that surface crevasses propagate deeper in thick grounded glaciers and that the (compressive) seawater pressure acts as a stabilizing force retarding crack growth and preventing surface crevasses from penetrating as deeply into the ice as in the land terminated case. Again, this study leads us to the hypothesis that surface crevasse penetration alone is not sufficient to trigger iceberg calving, but it can lead to the faster flow of glaciers.

We next performed a sequence of experiments with marine terminating glaciers of thickness $h = 500$ m. We considered the extreme cases of the basal boundary condition: free slip (no basal friction) and no slip (frozen or fixed to the bed), where the former condition gives the upper bound on the depth to which crevasses penetrate while the latter boundary condition gives the lower bound. Additionally, the seawater depth is changed from $h_w = 0$ to $h_w = 0.5h$ to investigate the combined effect of water pressure and basal boundary condition. The curves of ice thickness normalized crack length versus time are given in Figure 11. The predicted equilibrium crevasse depth is $d = 0.6h$ when $h_w = 0.5h$ and $d = 0.94h$ when $h_w = 0$ with free slip at the base, whereas the equilibrium crevasse penetration depth is $d = 0.28h$ when $h_w = 0.5h$ and $d = 0.35h$ when $h_w = 0$ with no slip at the base. Thus, the basal boundary condition had a more prominent effect on the equilibrium crevasse depth than the water depth for $h_w = 0.5h$ illustrating the importance

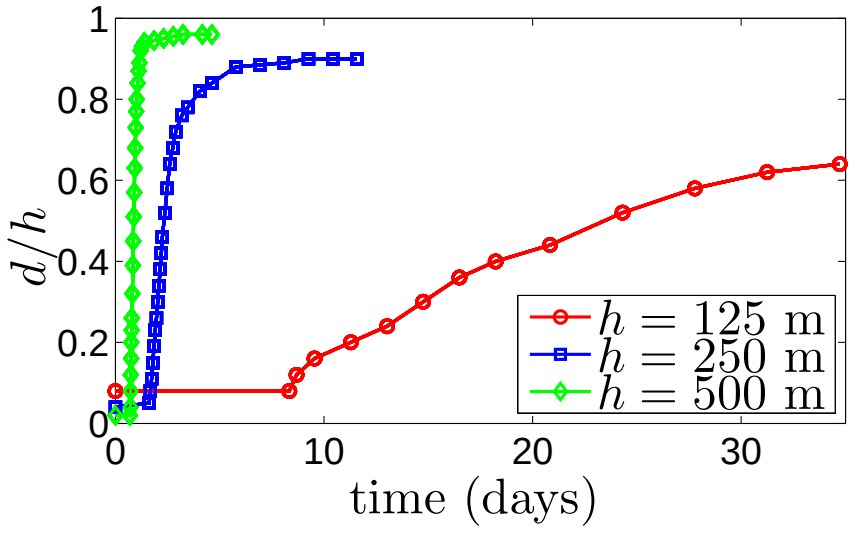

Figure 9: Curves of crevasse depth (d) normalized with slab thickness (h) versus time, for ice slabs of thickness $h = 125, 250, 500$ m when $h_w = 0$. Results indicate that crevasses only penetrate (nearly) the entire thickness in thicker glaciers.

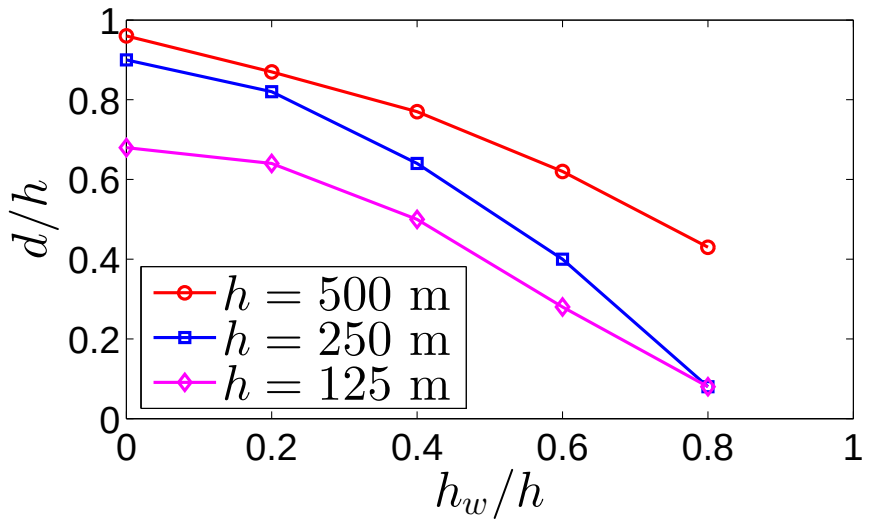

Figure 10: Fraction of the ice slab penetrated by surface crevasses (d/h) as a function of the ratio of seawater depth (h_w) to ice slab thickness (h).

of the sliding law in determining crevasse penetration depths. In Figure 11, we also compared the equilibrium crevasse depth estimated directly from crack growth simulations with that from the Nye zero-stress model [34]. To determine the Nye crevasse depths, we simulated the stress field in notched rectangular ice slabs due to viscoelastic deformation without any creep damage evolution and then found the depths at which the longitudinal stress vanishes. We found that the Nye zero stress model predicted shallower crevasses compared to the direct crack growth simulations, illustrating the important role played by creep damage evolution and stress concentration effects in the fracture of glaciers.

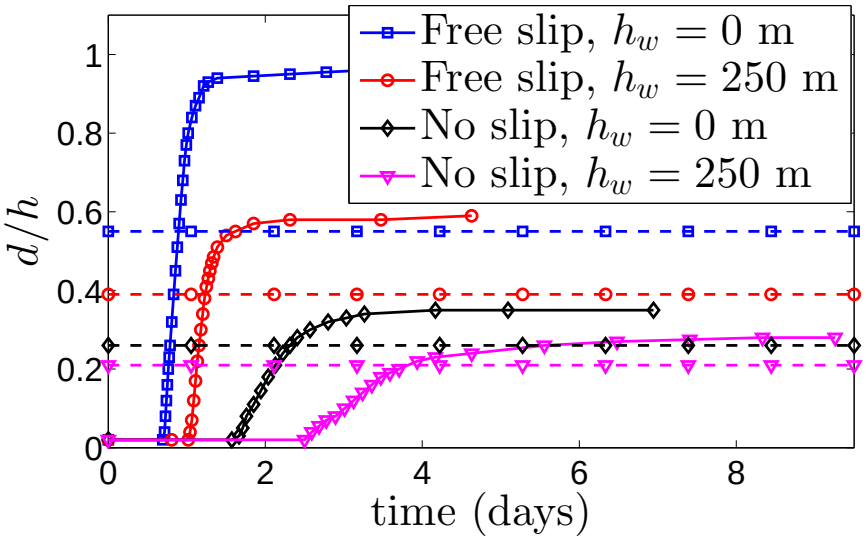

Figure 11: Curves of normalized crack length (d/h) versus time showing the effect of hydrostatic pressure and basal boundary condition on crevasse propagation. The corresponding Nye depths are marked by dashed horizontal lines.

Size of icebergs In the previous set of experiments we initialized our simulations using a notch at the mid-length at the top surface. We also investigated the most favorable location for crevasse initiation and subsequent propagation in glaciers that is closest to the terminus as a function of the applied/assumed boundary conditions. Since crevasse propagation is driven by tensile stresses, we assume that the location of maximum tensile stress $l_{\max}$ that is closest to the terminus is the most favorable location for crevasse initiation. The distance $l_{\max}$ gives us an estimate of the size of the calving icebergs as a function of the boundary conditions. In the simulation experiments, we considered an ice slab of thickness $h = 500$ m and varied the water depth from $h_w = 0$ to $h_w = 0.8h$. From the simulation result shown in Figure 12, we can see that as the water depth h_w increases the distance $l_{\max}$ decreases. The results suggest that for a dry glacier ($h_w = 0$) the iceberg size is $l_{\max} > 2h$, whereas for a marine terminating glacier with $h_w = 0.5h$ the iceberg size $l_{\max} < h$. This suggests that glaciers terminating in deep water would generate smaller icebergs than those grounded in shallow water. We also investigated the effect of the basal boundary condition. We performed full creep fracture simulations assuming free slip and no slip conditions on two identical ice slabs with two initial notches placed at distances less than and greater than the thickness of the slab from the terminus (right edge). The results shown in Figure 13 indicate that the crack farther

away from the terminus grows under free slip basal conditions; whereas the nearer crack grows under fixed basal conditions. This study suggests that basal boundary conditions and seawater depth both play a prominent role in determining the size of the calving icebergs by establishing favorable locations for crevasse propagation.

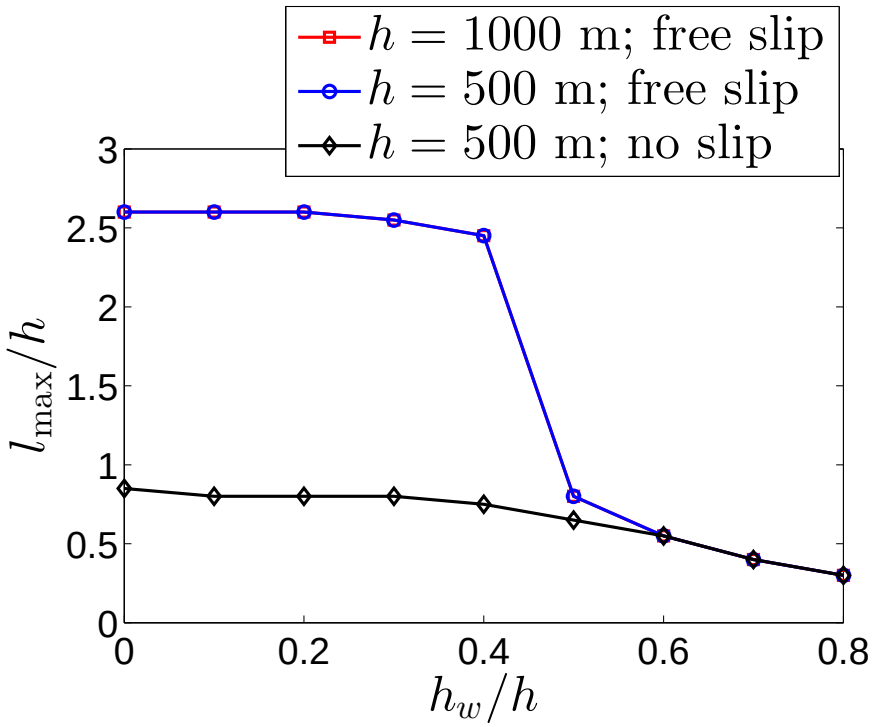

Figure 12: Normalized distance of maximum tensile stress from the terminus ($l_{\max}/h$) varies as a function of the seawater depth ratio (h_w/h).

3.1.4 Summary

We have developed a 3D continuum damage model for the temperature dependent creep response of polycrystalline ice under a multiaxial state of stress. The viscoelastic constitutive model captures the nonlinear viscous behavior of polycrystalline ice that constitutes glaciers, ice-sheets and ice-shelves. The constitutive model is coupled with a meso-scale damage model that accounts for the material degradation at low stresses ranges (< 1.0 MPa). All model parameters of this visco-elastic damage model are calibrated using published data of uniaxial tension tests [31] and uniaxial compression tests [29, 23]. The model predictions are then compared to experimental data from constant strain-rate tests including uniaxial tests [29] and biaxial tests [35, 36]. They are also compared to previous numerical results of triaxial tests [25, 37]. The predictions are consistent with both experimental and numerical results in the literature.

By employing the viscoelastic constitutive damage model, we have also studied surface crack propagation in grounded slabs of ice. Our results suggest that surface crevasses propagate deeper in thicker grounded glaciers and seawater pressure retards surface crevasse propagation. The basal boundary condition and seawater depth not only affect the crevasse propagation rate, but also affect the favorable location for surface crevasse formation. Our study suggests that crevasses form closer

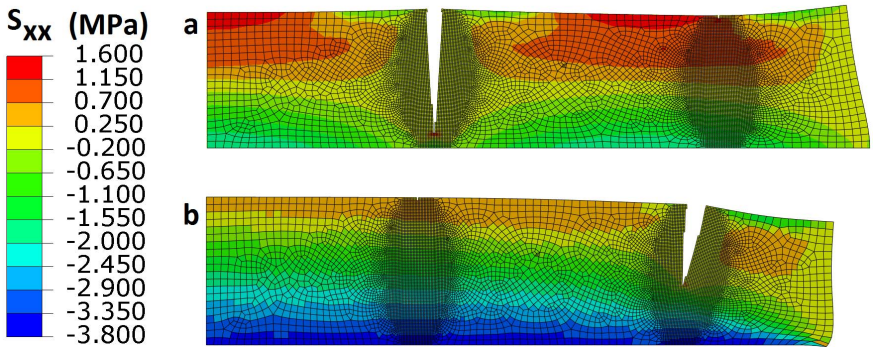

Figure 13: Contour plots of the longitudinal stress in x direction (in MPa) showing different preferred locations for crevasse opening with: (a) free slip at the base; (b) no slip (fixed) at the base. The deformations and crack opening displacements are not drawn to scale.

to the terminus when the seawater depth is larger or when the glacier base is fixed to the bedrock, highlighting the important role basal sliding plays in iceberg calving. Our computations suggest that crevasses can propagate deeper than those predicted by the Nye zero stress model, illustrating the dominant role of creep damage (fracture) evolution. However, even in the case of dry thick glaciers, water-free surface crevasses do not propagate the full glacier thickness. This suggests that melt-water pressure driven surface crevasse propagation or seawater pressure driven basal crevasse propagation may be plausible mechanisms that lead to the break-up of glaciers. The main advantage of our computational model is that it is not constrained by any simplistic assumptions and it can help consider realistic scenarios so as to gain new insights into the processes leading to ice fracture and glacial calving.

For more results and discussions the reader is referred to the following published work [9, 10, 12, 11].

3.2 Progress with modeling fracture using extended finite elements

3.2.1 Brief introduction to the Extended finite element method

The ice shelf model described in the previous section gives a general description of how critical stress sections are generated and propagated but cannot model the fracture explicitly. Modeling cracks as they propagate in solids is a severe limitation of conventional finite elements as re-meshing is not a trivial task, in particular if many cracks are interacting and propagating at the same time. The situation is further complicated by the addition of "double nodes" (two nodes sharing the same spatial point) along the crack line which is often needed to facilitate crack opening. This limitation may be circumvented by the extended finite element approach which allows one to employ regular meshes to model cracks and holes. The extended finite element method (XFEM) offers great flexibility in modeling weak and strong discontinuities [38, 39]. XFEM alleviates the need for meshing the domain such that it is aligned with the discontinuities modeled, and consequently standard structured or unstructured meshes may be employed. The key idea of XFEM is to locally enrich the standard FEM approximation with local partition of unity enrichment functions chosen according to the physics of the problem at hand. As a result, discontinuities may not only be better approximated, but also geometrical features (e.g. cracks, holes and inclusions) can

be separated from mesh generation. For crack problems, two types of enrichment functions are typically used: Branch functions for nodes associated with tip elements, and a Heaviside function for element nodes fully cut by the crack.
Consider a domain $\Omega \subset \mathbf{R}^n$ $(n = 1, 2, 3)$, discretized by N_{el} elements. The approximated displacement field $u^h(x)$ via extended finite elements is given by

$$u^h(x) = \sum_{I \in N} N_I(x) u_I + \sum_{J \in N_{cr}} N_J(x)(H(x) - H(x_J))a_J + \sum_{K \in N_{tip}} N_K(x) \sum_{\alpha=1}^{4} (F_\alpha(x) - F_\alpha(x_K))b_{\alpha K} \tag{12}$$

where, N_I and u_I are the standard shape functions and the displacement solution with respect to node I, respectively. N is the set of all nodes. $H(x)$ is the Heaviside step function given by

$$H(x) = \begin{cases} 1 & x \geq 0 \\ -1 & x < 0 \end{cases} \tag{13}$$

and used to enrich all element nodes cut by the crack (element behind the crack tip denoted by the nodal set N_{cr}), as illustrated in Figure 14 (nodes enriched by the function $H(x)$ are often referred to as jump enriched nodes and are marked by circles in Figure 14). a_J are the additional degrees of freedom added to the jump enriched nodes. F_α are the Branch functions given by

$$F_\alpha(r, \theta)_{\alpha=1,2,3,4} = \{\sqrt{r}\sin\frac{\theta}{2}, \sqrt{r}\cos\frac{\theta}{2}, \sqrt{r}\sin\frac{\theta}{2}\sin\theta, \sqrt{r}\cos\frac{\theta}{2}\sin\theta\} \tag{14}$$

where r is the distance between any point in the mesh to the crack tip and θ is the angle to the crack tip in local crack coordinates. These Branch functions are used to enrich tip element nodes denoted by the nodal set N_{tip} (In Figure 14, the crack tip nodes are marked by squares), and $b_{\alpha K}$ are the additional degrees of freedom added to tip elements. Multiplication of the Heaviside function and the Branch functions by the standard shape function is used to obtain the partition of unity property.

Figure 15 depicts the implementation of XFEM on a multiple crack problem and the corresponding stresses.

3.3 Inexact Schwarz-AMG preconditioners for crack problems modeled by XFEM

Traditional algebraic multigrid (AMG) preconditioners are not well suited for crack problems modeled by extended finite element methods (XFEM). This is mainly due to the unique XFEM formulations which embed discontinuous fields in the linear system by addition of special degrees of freedom. These degrees of freedom are not properly handled by the AMG coarsening process and lead to slow convergence.
In the paper [16] we propose a simple domain decomposition approach that retains the AMG advantages on well behaved domains by avoiding the coarsening of enriched degrees of freedom. The idea is to employ a multiplicative Schwarz preconditioner where the physical domain is partitioned into a "healthy" (or unfractured) and "cracked" subdomains. The "healthy" subdomain, containing only standard degrees of freedom, is solved approximately by one AMG V-cycle, followed by

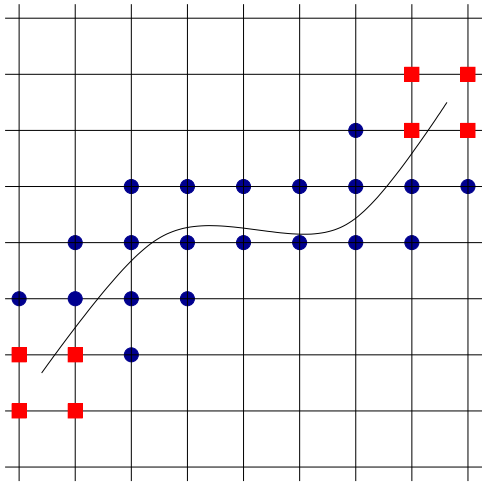

Figure 14: Enriched nodes in the extended finite element method for a given crack. Circles denote nodes enriched by the Heaviside (jump) function and squares denote the tip element nodes enriched by Branch functions.

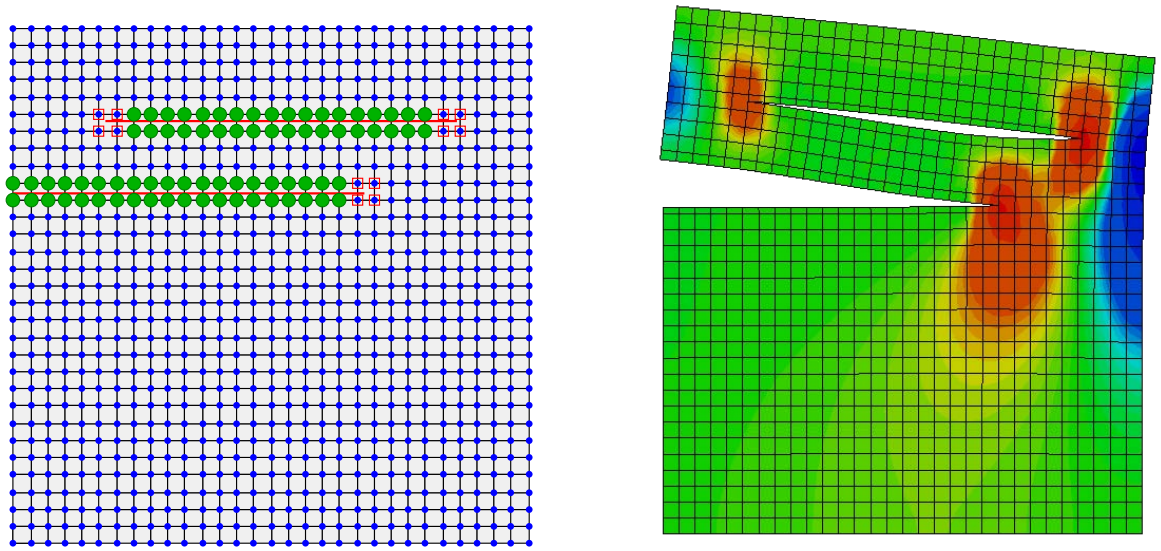

(a) (b)

Figure 15: (a) Enriched Heaviside and branch nodes. (b) stresses σ_{yy}

concurrent direct solves of "cracked" subdomains. This strategy alleviates the need to redesign special AMG coarsening strategies that can handle XFEM discretizations. Numerical examples on various crack problems clearly illustrate the superior performance of this approach over a brute force AMG preconditioner applied to the linear system.

3.3.1 General Methodology

The proposed multiplicative Schwarz preconditioner begins with a special domain decomposition. As shown in Fig. 16, we consider two possible partitioning strategies: (i) a single subdomain containing all cracks (see Fig. 16(a)) and (ii) multiple crack subdomains (see Fig. 16(b)), where each crack owns its own subdomain. In many cases the physics of the problem will determine the partitioning scheme. For example, clusters of cracks and microcracks, e.g., formed due to a localized impact or indentation loads, can be aggregated into a single subdomain, while more isolated cracks, nucleating at far distances from each other, e.g. formed due to fatigue loads applied to the whole structure, may be too far apart and will require their own subdomains. In any case, the two strategies lead to the same type of systems.

In Fig. 16, we refer to the subdomain Ω_1^h that does not contain any enriched nodes (or cracks) as a "*healthy*" subdomain (for simplicity of the presentation we will only consider one *healthy* subdomain). The other subdomains containing at least one crack, and hence all enriched degrees of freedom associated with that crack, are referred to as "*cracked*" subdomains and denoted by Ω_i^c. *Cracked* subdomains may also contain one or several layers of elements around cracks that constitute the overlap with the *healthy* subdomain.

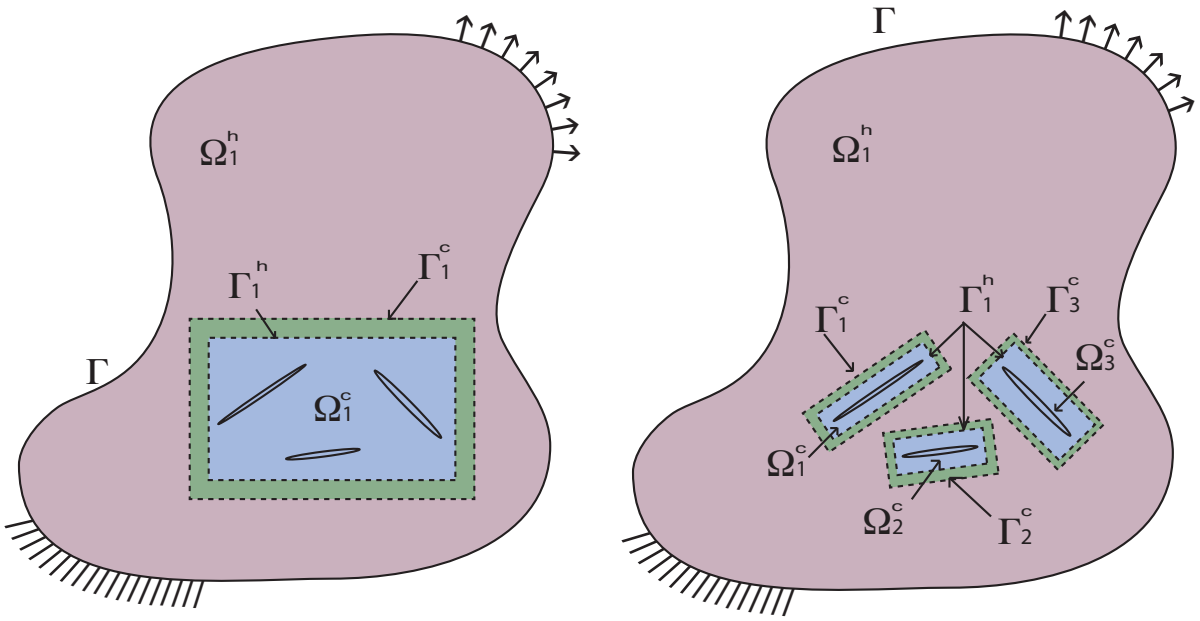

Figure 16: Schematic representation of the "*healthy*" and "*cracked*" subdomains in the formulation of domain decomposition. [a] multiple cracks share a single *cracked* subdomain [b] each crack is assigned to a different *cracked* subdomain.

The general formulation leads to a coupled set of linear systems associated with the *healthy* and *cracked* subdomains. The coupling occurs through the boundary conditions and overlapping elements. Note that in this formulation, *cracked* subdomains are decoupled from each other and are only coupled to the *healthy* subdomain. This property is not an essential feature of the proposed approach, but is adopted in the current work to keep the description of the method simple, without any loss of generality.

Preconditioner setup and algorithm flow: Our proposed approach uses a domain decomposition algorithm with an inexact multiplicative Schwarz method as the preconditioner for the residual obtained at each iteration of a global GMRES solver. This partitioning is only performed once and is reused over successive iterations. The *healthy* subdomain is approximately solved using one AMG V-cycle and *cracked* subdomains are solved concurrently with a direct solver. The two solutions are then assembled back to be returned to the global GMRES solver. A schematic representation of the algorithm is illustrated in Fig. 17 and shown in a condensed form in Fig. 18.

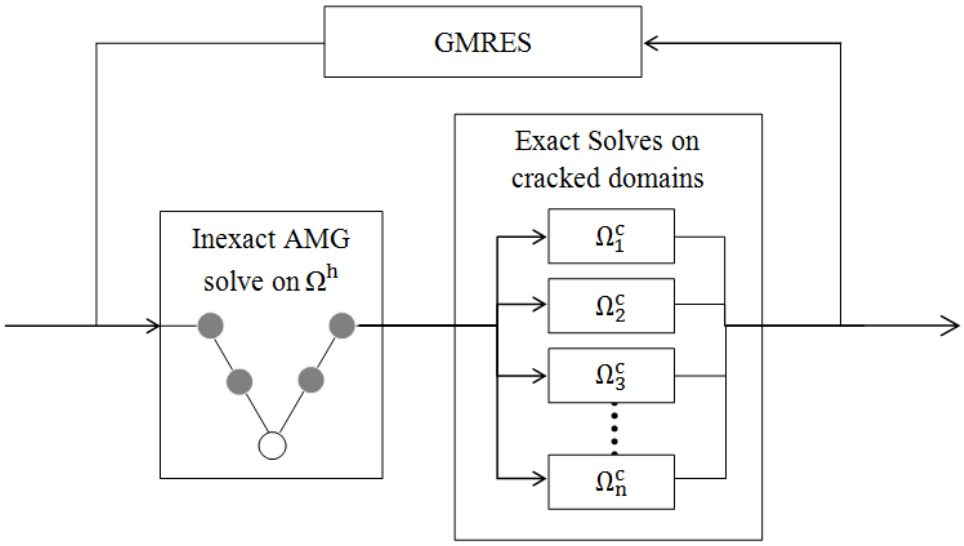

Figure 17: Schematic description of the inexact Schwarz-AMG preconditioner .

While one could argue that the use of a direct solver on the *cracked* subdomains may be computationally too expensive, we point out that *cracked* subdomains are relatively small compared to the overall size of the problem and therefore, this step is fairly inexpensive. Moreover, linear systems associated with *cracked* subdomains are factored before starting GMRES iterations, and reused in successive iterations of the preconditioner.

Step 1: Apply one AMG V cycle to the *healthy* subdomain

$$\boldsymbol{u}^h \leftarrow AMG(\boldsymbol{r}^h, \boldsymbol{K}^h) \text{ for the healthy subdomain}$$

Step 2: solve all *cracked* subdomains

$$\boldsymbol{u}_i^c \leftarrow \mathrm{B}_i(\boldsymbol{r}^h - \boldsymbol{K}^h \boldsymbol{u}^h) \text{ for all } \textit{cracked} \text{ subdomains } i$$

Step 3: Update the residual and return to the GMRES solver

$$\boldsymbol{u} \leftarrow assemble(\boldsymbol{u}^h, \boldsymbol{u}_1^c, \ldots, \boldsymbol{u}_n^c)$$

Figure 18: GMRES preconditioned by an inexact Schwarz-AMG preconditioner.

One of the great interests of this process is that it is utterly simple to implement and provides a way to apply the AMG method to the bulk of the domain, retaining its convergence properties for crack problems modeled by XFEM.

3.3.2 Numerical examples

Numerical results comparing the inexact Schwarz-AMG preconditioner versus a brute force AMG preconditioner within GMRES are provided in this section. In this report we only present two examples, however for more results the reader is referred to [16, 18]. A brute force AMG method is defined as an AMG method that is directly applied to the entire domain without redesigning the AMG to take into account enriched degrees of freedom. The AMG method employed in our studies is the one based on smoothed aggregation concepts and has been implemented in the MueMat package at Sandia Labs.

Crack growth under pure mode I loading: The first example compares the convergence of the AMG brute force preconditioner to the one obtained by the inexact Schwarz-AMG preconditioner as a function of increasing crack size. The inexact Schwarz-AMG preconditioner is a multiplicative Schwarz method in which the *healthy* subdomain is approximated with a single AMG cycle, and the *cracked* subdomain is solved exactly. Note that in this problem the *cracked* subdomain grows and follows the crack path as it propagates in the domain. The problem considered is a square plate with dimensions of $1 \times 1\ [m]$, and a crack propagating in mode I from one end to the other end of the plate. As shown in Fig. 19(a), a uniformly distributed tensile load of $1,000\ [N \cdot m^{-1}]$ applied to its top and bottom edges. Crack propagation is performed quasi-statically from an initial crack of length $a_{initial} = 0.12\ [m]$ to a final length of $a_{final} = 0.71\ [m]$. A mesh of 30×30 elements is chosen for this problem. Fig. 19(b) shows the number of iterations required by each method as a function of the crack length. This numerical experiment reveals that the inexact Schwarz-AMG preconditioner exhibits a faster convergence rate than the AMG brute force preconditioner but when the size of the crack increases the difference between the number of iterations needed by the two methods decreases.

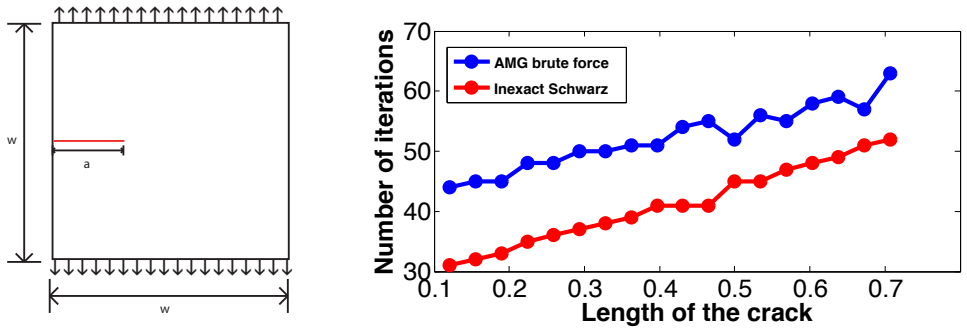

(a) (b)

Figure 19: Convergence of the preconditioners on the length growth problem. [a] geometric definition of the problem [b] number of iterations to converge as a function of crack length.

Multiple cracks with different lengths and orientations: In this example we investigate the convergence of the preconditioners on a plate containing three cracks of different lengths and orientations. Two strategies, illustrated in Fig. 16, are used to partition the domain into *healthy* and *cracked* subdomains. In the first case the *cracked* subdomain owns all the cracks (a single *cracked* subdomain) while in the second approach each crack owns its own local subdomain (multiple *cracked* subdomains). In addition an Additive Schwarz method is investigated and compared with the other methods. The plate dimensions, boundary conditions and loading is the same as given in Fig. 19(a). The mesh and the partitioned domains are shown in Fig. 20, and the convergence results are plotted in Fig. 21.
It is clear that both domain decomposition strategies give excellent results compared to the AMG brute force preconditioner. The AMG performance is poor, which is mainly attributed to the cracks having two sets of tip functions inside the domain, and in close proximity to each other. Moreover, the different orientation of the cracks makes it significantly harder for the AMG to generate appropriate aggregates and the coarsening of these special functions, significantly deteriorates its performance.

As expected, the multiplicative inexact Schwarz method with a single *cracked* subdomain gives slightly better performance than its counterpart with multiple *cracked* subdomains. The single *cracked* subdomain has converged in 50 iterations whereas it converged in 63 iterations when multiple subdomains are introduced. This behavior is due to the fact that all the cracks are solved concurrently in the single *cracked* subdomain case whereas solving them in a sequential manner introduce a small delay in the coupling of these cracks.

Summary The paper presents an inexact Schwarz-AMG preconditioning approach for crack problems modeled by XFEM, in order to retain the convergence properties of smoothed aggregation AMG for elastostatic problems. The preconditioner is based on the domained partition into "healthy" (or unfractured part), and a "cracked" part that includes all the XFEM enriched degrees of freedom. While the solution in the "healthy" subdomain is approximated inexactly by a single multigrid V-cycle, the "cracked" subdomains (single or multiple) are solved exactly. This alleviates the need to redesign the AMG coarsening algorithms to handle enriched degrees of freedom.

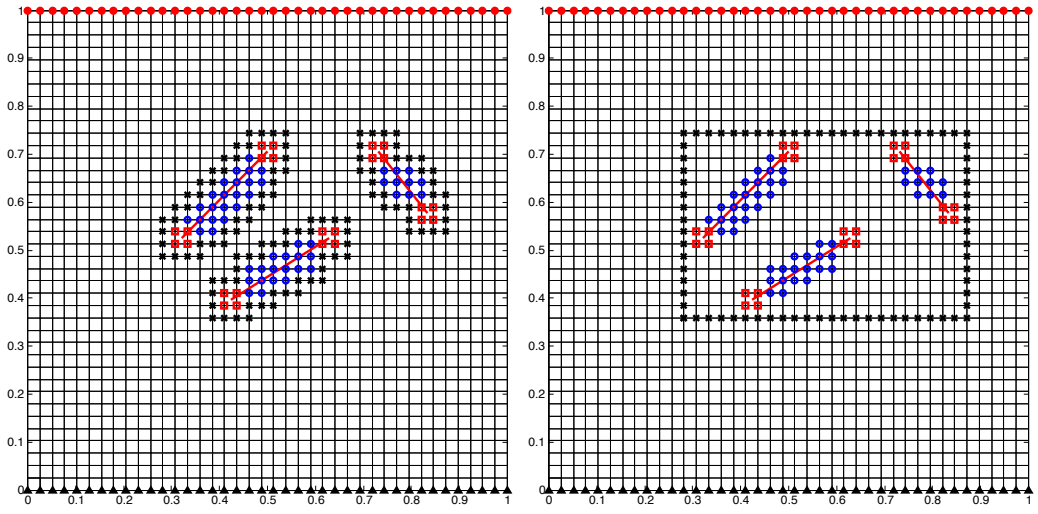

(a) (b)

Figure 20: Domain decomposition and mesh of a plate with three cracks with different lengths and orientations [a] Decomposition with multiple *cracked* subdomains [b] Decomposition with a single *cracked* subdomain.

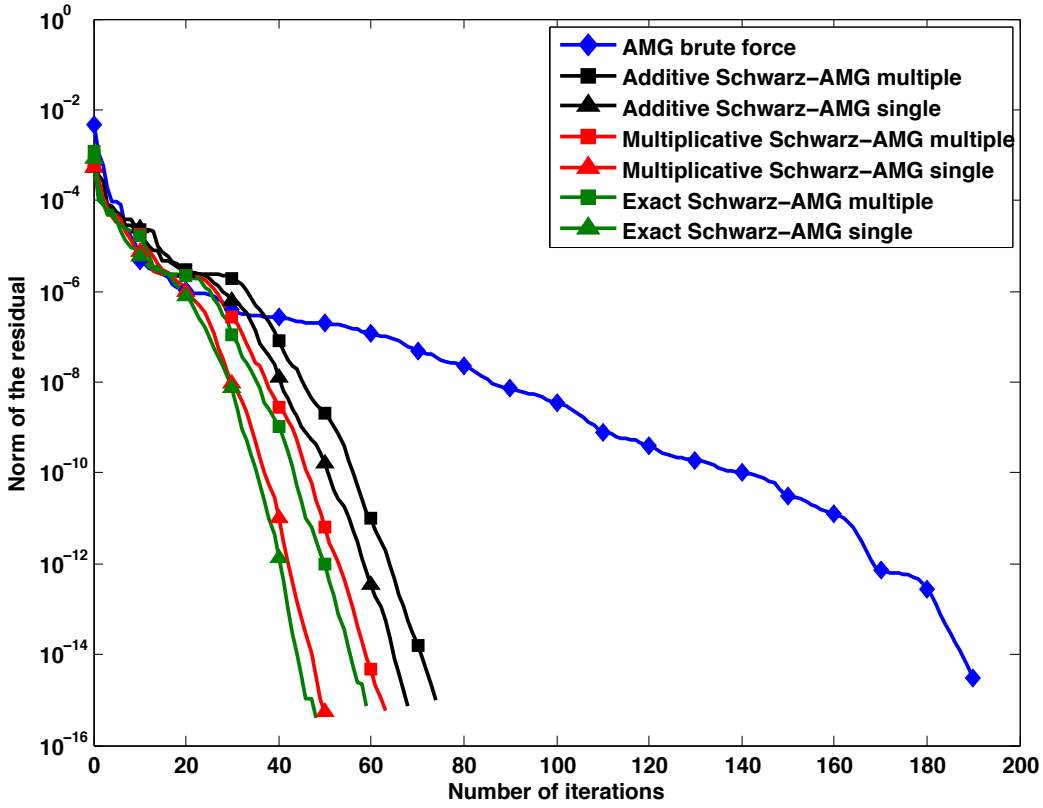

Figure 21: Comparison of the convergence rate for the decomposition strategies shown in Fig. 20.

Table 1: Summary of the convergence results for the problem considered in Fig. 20.

	AMG brute force	Additive Schwarz-AMG	Multiplicative Schwarz-AMG	Exact Schwarz-AMG
Single "crack" subdomain	190	68	50	48
Multiple "crack" subdomains	190	74	63	59

Numerical examples on various crack problems clearly illustrate the superior performance of this approach over a brute force AMG preconditioner, in particular when multiple random cracks are fully embedded in the structure. This is one approach to apply AMG schemes to XFEM problems with no adjustments of the original method. For more details the reader is referred to [16, 18].

4 Papers published under this DOE funding

The following papers are associated with this funding and have been already published, submitted for publication, or are in preparation:

[A1] Haim Waisman, *The extended stiffness derivative technique to extract the strain energy release rates*, proceedings of the 16^{th} US National Congress of Theoretical and Applied Mechanics, State College, Pa, June 2010.

[A2] Xia Liu and Haim Waisman, *Computationally efficient micro crack modeling in statics and dynamics based on simplified crack tip enrichments within the extended finite element method*, proceedings of the 16^{th} US National Congress of Theoretical and Applied Mechanics, State College, Pa, June 2010.

[A3] Haim Waisman, *An analytical stiffness derivative extended finite element technique for extraction of crack tip Strain Energy Release Rates*, Engineering Fracture Mechanics 77 (16):3204-3215, 2010.

[A4] Xia Liu, Haim Waisman and Jacob Fish, *A New Crack Tip Enrichment Function in the Extended Finite Element Method for General Inelastic Materials*, Accepted for publication, International Journal for Multiscale Computational Engineering (2011).

[A5] Ravindra Duddu and Haim Waisman, *A temperature dependent creep damage model for polycrystalline ice*, Mechanics of Materials 46: 23-41,2012.

[A6] Badri Hiriyur, Ray Tuminaro, Haim Waisman, Erik Boman and David Keyes *A Quasi-Algebraic Multigrid Approach to Fracture Problems Based on Extended Finite Elements*, SIAM Journal on Scientific Computing 34(2):A603-A626, 2012.

[A7] Luc Berger-Vergiat, Haim Waisman, Badri Hiriyur, Ray Tuminaro and David Keyes, *Inexact Schwarz-AMG preconditioners for crack problems modeled by XFEM*, International Journal for Numerical Methods in Engineering 90(3):311-328, 2012.

[A8] Ravindra Duddu and Haim Waisman, *A nonlocal continuum damage mechanics approach to simulation of creep fracture in ice-sheets*, Computational Mechanics, 51(6):961-974, 2013.

[A9] Axel Gerstenberger and Ray Tuminaro, *An algebraic multigrid approach to solve extended finite element method based fracture problems*, International Journal for Numerical Methods in Engineering 94(3):248–272, 2013.

[A10] Ravindra Duddu, Jeremy Bassis and Haim Waisman, *A numerical investigation of surface crevasse propagation in glaciers using nonlocal continuum damage mechanics*, Geophysical Research Letters 40(12):3064-3068, 2013.

[A11] Ravindra Duddu and Haim Waisman, *On the continuum damage mechanics approach to modeling of polar ice fracture: A reply*, Journal of Glaciology, 59(216), 2013.

[A12] Haim Waisman and Luc Berger-Vergiat, *An adaptive domain decomposition preconditioner for crack propagation problems modeled by XFEM*, Accepted, International Journal for Multiscale Computational Engineering (2013).

5 Future Plans

While significant progress has been made there is still much to be done to close the knowledge gap on fracture of ice sheets and ice shelves. We have recently submitted an NSF proposal (currently pending) on simulating iceberg calving from ice shelves using the damage mechanics model which was developed in this project. Thus, we feel that this project is a significant milestone in understanding and modeling the fracture of ice sheets and ice shelves.

The NSF proposed work, which builds upon this DOE project is as follows:

Mass loss from the Antarctic Ice Sheet occurs primarily through its ice shelves, which are floating platforms of ice that extend into the ocean and surround the Antarctic ice sheet. Because of the cold atmospheric temperatures, most of this mass loss comes from the combination of the detachment of icebergs (calving) and the gradual erosion of ice by basal melting. The challenge in predicting future ice sheet mass loss, however, is that many of the processes associated with ice shelf demise remain poorly understood. Although progress has been made in our understanding of basal melting, a quantitative understanding of iceberg calving from ice shelves remains elusive. This is partly because calving requires that we understand and simulate the three-dimensional initiation and propagation of fractures within the ice over timescales that range from seconds to decades (or longer). Our primary objective is thus to improve our knowledge of iceberg calving using a multi-faceted approach that addresses: (i) the physics of fracture initiation and propagation using a continuum creep damage mechanics model that can simulate the time-dependent visco-elastic failure of ice and; (ii) the thermo-mechanical evolution of fractures after inception due to freeze-on and melting induced excavation of fractures. Both facets of our proposal are challenging and computationally demanding so that concurrent fracture simulation in tandem with global ice sheet

modeling will be prohibitively expensive and complicated, even with the latest parallel computing platforms. Therefore, we propose to use our damage model to test existing parameterizations of iceberg calving and seek improved representations of fracture propagation and iceberg calving that can be more easily ingested into existing numerical ice sheet or ice shelf models.

Iceberg calving rates provide boundary conditions to global ice sheet models and thus are extremely important. However, current models rely on empirical assumptions that are simplistic and therefore cannot predict accurate rates due to global warming and other accelerating processes. Our proposed fracture mechanics model will provide a physically based computational framework that can be used to simulate iceberg calving from ice shelves. Moreover, given the fundamental nature of this proposal and departure from current theories, especially our focus on thermodynamic evolution of fractures, it is likely that new physics related to ice calving will be discovered and knowledge about its overall effect on global climate will be gained.

The key socio-economic impact of this proposed work will be realized through the insights it provides into the dynamics of ice shelves and their contribution to the freshwater budget and mass budget of the Antarctica ice sheet in the coming centuries. The knowledge gained will impact the field of glaciology, fracture mechanics and applied mathematics through the development of novel translational methods for studying the multi-physics and multi-scale fracture of materials. Our broader educations efforts also target education at the elementary school, high school, undergraduate and graduate level with students at the latter two levels incorporated into our research efforts.

6 Unexpended funds

Funding has being used to support students, a postdoc, PI's summer salary, travel and software. Currently all the funding has been spent.

References

[1] AFP. Huge ice shelf breaks from antarctica, fractures. *Discovery News Channel*, April 28, 2009.

[2] A. Shepherd, D. Wingham, T. Payne, and P. Skvarca. Larsen ice shelf has progressively thinned. *Science*, 302(5646):856–859, October 31, 2003.

[3] D. Ljunggren. Giant chunks break off canadian ice shelf. *Reuters*, Jul 29, 2008.

[4] S. M. Jepsena, E. E. Adamsa, and J. C. Priscub. Fuel movement along grain boundaries in ice. *Cold Regions Science and Technology*, 45(3):158–165, 2006.

[5] K. J. Bird and D. W. Houseknecht. Sizing up oil on alaskas north slope. *GeoTimes*, November 2006.

[6] Z. P. Bazant. Large-scale thermal bending fracture of sea ice plates. *Journal of geophysical research*, 97:739–751, 1992.

[7] J. Weiss and M. Gay. Fracturing of ice under compression creep as revealed by a multifractal analysis. *Journal of geophysical research*, 103(B10):2400524016, 1998.

[8] P. B. Price. A habitat for psychrophiles in deep antarctic ice. *Proceedings of the National Academy of Sciences of the United States of America*, 97:1247–1251, 2000.

[9] R. Duddu and H. Waisman. A temperature dependent creep damage model for polycrystalline ice. *Mechanics of Materials*, 46:23–41, 2012.

[10] R. Duddu and H. Waisman. A nonlocal continuum damage mechanics approach to simulation of creep fracture in ice-sheets. *Computational Mechanics*, 51:961–974, 2013.

[11] R. Duddu and H. Waisman. On the continuum damage mechanics approach to modeling of polar ice fracture: A reply. *Journal of Glaciology*, 59(216), 2013.

[12] R. Duddu, J. Bassis, and H. Waisman. A numerical investigation of surface crevasse propagation in glaciers using nonlocal continuum damage mechanics. *GRL*, 40(12):3064–3068, 2013.

[13] R. Duddu, H. Waisman, J.N. Bassis, and R. Tuminaro. A viscoelastic continuum damage model for creep fracture in ice sheets. Poster, presented at the World Climate Research Programme Open Science Meeting (WCRPOSC), Denver, CO. Oct 24-28, 2011.

[14] R. Duddu, H. Waisman, J.N. Bassis, and R. Tuminaro. A nonlocal continuum damage mechanics approach to simulation of creep and fracture in ice sheets. Poster, presented at the American Geophysical Union Fall Meeting, San Francisco, CA. Dec 5-9, 2011.

[15] B. Hiriyur, R. Tuminaro, H. Waisman, E. Boman, and D. Keyes. A quasi-algebraic multigrid approach to fracture problems based on extended finite elements. *SIAM Journal of Scientific Computing*, 34(2):A603–A626, 2012.

[16] L. Berger-Vergiat, H. Waisman, B. Hiriyur, R. Tuminaro, and D. Keyes. Inexact schwarz-amg preconditioners for crack problems modeled by xfem. *International Journal for Numerical Methods in Engineering*, 90(3), 2012.

[17] A. Gerstenberger and R. Tuminaro. An algebraic multigrid approach to solve extended finite element method based fracture problems. *International Journal for Numerical Methods in Engineering*, 94(3):248–272, 2013.

[18] H. Waisman and L. Berger-Vergiat. An adaptive domain decomposition preconditioner for crack propagation problems modeled by xfem. *Accepted, International Journal for Multiscale Computational Engineering*, 2013.

[19] X. Liu and H. Waisman. Computationally efficient micro crack modeling in statics and dynamics based on simplified crack tip enrichments within the extended finite element method. In *proceedings of the* 16^{th} *US National Congress of Theoretical and Applied Mechanics*, State College, Pa., June, 2010.

[20] X. Liu, H. Waisman, and J. Fish. A new crack tip enrichment function in the extended finite element method for general inelastic materials. *Accepted for publication, International Journal for Multiscale Computational Engineering*, 2011.

[21] H. Waisman. The extended stiffness derivative technique to extract the strain energy release rates. In *proceedings of the* 16^{th} *US National Congress of Theoretical and Applied Mechanics*, State College, Pa., June, 2010.

[22] H. Waisman. An analytical stiffness derivative extended finite element technique for extraction of crack tip strain energy release rates. *Engineering Fracture Mechanics*, 77:3204–3215, 2010.

[23] Jacka T. H. The time and strain required for development of minimum strain rates in ice. *Cold Regions Science and Technology*, 8(3):261–268, 1984.

[24] Sinha N. K. Elasticity of natural types of polycrystalline ice. *Cold Regions Science and Technology*, 17(2):127–135, 1989.

[25] D. G. Karr and K. Choi. A three-dimensional constitutive damage model for polycrystalline ice. *Mechanics of Materials*, 8(1):55–66, 1989.

[26] J. W. Glen. The creep of polycrystalline ice. *Proceedings Of The Royal Society Of London Series A-Mathematical And Physical Sciences*, 228(1175):519–538, 1955.

[27] S. Murakami. Notion of continuum damage mechanics and its application to anisotropic creep damage theory. *Journal of Engineering Materials and Technology - Transactions of the ASME*, 105(2):99–105, 1983.

[28] A. Pralong and M. Funk. Dynamic damage model of crevasse opening and application to glacier calving. *Journal of Geophysical Review - Solid Earth*, 110(B1):B1309, 2005.

[29] M. Mellor and D. M. Cole. Deformation and failure of ice under constant stress or constant strain-rate. *Cold Regions Science and Technology*, 5(3):201–219, 1982.

[30] S. Murakami and N. Ohno. A continuum theory of creep and creep damage. *paper presented at 3rd Symposium Creep in Structures, International Union of Theoretical and Applied Mechanics, Leicaster, U. K.*, 1980.

[31] O. Mahrenholtz and Z. Wu. Determination of creep damage parameters for polycrystalline ice. *paper presented at Third International Conference on Ice Technology, Advances in Ice Technology, Massachusetts Institute of Technology, Cambridge, MA*, 1992.

[32] J. N. Bassis and C. C. Walker. Upper and lower limits on the stability of calving glaciers from the yield strength envelope of ice. *Proceedings of the Royal Society A*, 468:913–931, 2012.

[33] D.I. Benn, N.R.J. Hulton, and R.H. Mottram. Calving laws, sliding laws and the stability of tidewater glaciers. *Annals of Glaciology*, 46(1):123–130, 2007.

[34] JF Nye. The Distribution of Stress and Velocity in Glaciers and Ice-Sheets. *Proceedings of the Royal Society of London. Series A, Mathematical and Physical Sciences*, 239(1216):113–133, 1957.

[35] E. M. Schulson and O. Y. Nickolayev. Failure of columnar saline ice under biaxial compression - failure envelopes and the brittle-to-ductile transition. *Journal of Geophysical Review - Solid Earth*, 100(B11):22383–22400, 1995.

[36] E. M. Schulson and S. E. Buck. The ductile-to-brittle transition and ductile failure envelopes of orthotropic ice under biaxial compression. *Acta Metallurgica Et Materialia*, 43(10):3661–3668, 1995.

[37] Z. Wu and O. Mahrenholtz. Creep and creep damage of polycrystalline ice under multi-axial variable loading. *paper presented at 12th International Conference on Offshore Mechanics and Arctic Engineering, American Society of Mechanical Engineers, Glasgow, U.K.*, 1993.

[38] T. Belytschko and T. Black. Elastic crack growth in finite elements with minimal remeshing. *International Journal for Numerical Methods in Engineering*, 45:601–620, 1999.

[39] N. Moës, J. Dolbow, and T. Belytschko. A finite element method for crack growth without remeshing. *International Journal for Numerical Methods in Engineering*, 46:131–150, 1999.